Construction and Building Materials 220 (2019) 1–9

Contents lists available at ScienceDirect

Construction and Building Materials

journal homepage: www.elsevier.com/locate/conbuildmat

Shrinkage properties of concretes using blast furnace slag and frost-resistant accelerator

Hyeonggil Chol [a], Juncheol Lee [b,*], Bokyeong Lee [c], Jeongsoo Nam [d]

[a] School of Architecture, Kyungpook National University, Daegu, Republic of Korea
[b] Daegyeong Regional Infrastructure Technology Development Center, Kyungpook National University, Daegu, Republic of Korea
[c] Intelligent Construction Automation Center, Kyungpook National University, Daegu, Republic of Korea
[d] Department of Architectural Engineering, Chungnam National University, Daejeon, Republic of Korea

HIGHLIGHTS

- Shrinkage properties of concrete using blast furnace cement with a frost-resistant accelerator were evaluated.
- Shrinkage strain and cracking potential was increased with the addition of frost-resistant accelerator.
- Change in 20–30 nm and ink-bottle pore volume was large effect on the shrinkage properties of concrete.

ARTICLE INFO

Article history:
Received 28 March 2019
Received in revised form 25 April 2019
Accepted 1 May 2019
Available online 3 June 2019

Keywords:
Blast furnace slag cement
Frost-resistant accelerator
Shrinkage
Cracking
Pore volume

ABSTRACT

This study investigated the shrinkage properties of concretes using blast furnace slag cement and frost-resistant accelerator as a construction technology in environmental-load-reducing cold weather concretes. The investigation results showed that as the frost-resistant accelerator was added to both Ordinary Portland Cement (OPC) and Blast Furnace Slag Cement (BB), the effect on the properties of fresh concrete was reduced and the compressive strength was increased from an early age. In addition, the free shrinkage strain and cracking potential at the same age tended to increase and the study result verified that the crack generation was also fast in the restrained condition. Meanwhile, the study results verified that the length of both of OPC and BB tended to increase upon adding the frost-resistant accelerator. Pore volume <30 nm diameter, in particular, 20–30 nm pore volume, and ink-bottle pore volume decreased such that the shrinkage volume increased, and the change in pore volume in this range was regarded as having a large effect on the shrinkage properties.

1. Introduction

The use of blast furnace slag cements has been expanded to reduce environmental load or employ industrial wastes efficiently. More recently, low heat and shrinkage-reduced blast furnace cement, which has a high content ratio of blast furnace slag, and Energy CO_2 Minimum (ECM) cements that achieve the Class C slag content ratio have been studied, but their use has been limited practically [1–3]. Although blast furnace slag cements have many advantages such as low heat, increased long-term strength, flame interruption performance, and suppression of the alkali–aggregate reaction, they also have drawbacks such as delayed early strength development and early frost damage during winter construction due to high temperature dependence, which is why much care must be taken when using blast furnace slag [4].

When concretes are used in winter, it is important that the concretes do not freeze until sufficient strength has been developed to prevent early frost damage due to the delayed strength development or freezing, and heat curing via temporary enclosure and use of a heater is typical [5–8]. However, the use of a temporary enclosure for concrete curing may cause CO_2 emissions due to the heater or warm curing in a space with extremely bad heat efficiency, which is why the use of a frost-resistant accelerator has increased to prevent early frost damage [9–14]. In particular, when the site conditions are difficult to install a temporary enclosure such as a steep slope or a strong wind, it is possible to perform the construction with a simple sheet curing by using a frost-resistant accelerator. The frost-resistant accelerator is an admixture developed to promote the hydration reaction of cement and to prevent the early frost damage after concrete pouring at low

* Corresponding author.
E-mail address: darkgreen@knu.ac.kr (J. Lee).

https://doi.org/10.1016/j.conbuildmat.2019.05.003
0950-0618/

temperature. This is due to the lowering of the freezing temperature of water in the concrete, and thus it belongs to anti-freezer. The effect of preventing the early frost damage caused by frost-resistant accelerator is not only due to the effect of freezing point depression but also hardening of the concrete [14].

Frost-resistant accelerator-mixed concretes can prevent fresh concretes from freezing at low temperature and develop the compressive strength required of concretes through performance improvement by accelerating the hardening and lowering the freezing point. Although frost-resistant accelerator is more expensive than other admixtures, it can shorten construction times or ensure economic feasibility as an effective means when special temporary facilities are required for temperature control and excessive exposure of construction members or when temperature control is difficult depending on the site conditions and construction circumstances [6,14]. Moreover, the strength improvement effect of frost-resistant accelerator due to hardening acceleration can overcome the drawbacks of early strength reduction during winter concrete construction, which is a shortcoming of blast furnace cements and why much attention has been paid to concretes that combine blast furnace cements with frost-resistant accelerators as environmental-load-reducing cold weather concreting technology [15]. However, most studies have focused on the strength restoration of Ordinary Portland Cement (OPC) as a base at an early age from the perspective of the prevention of early frost damage, but few studies have been conducted on the durability for long-term aging, in particular for shrinkage crack, which is the starting point of concrete deterioration. Since concrete cracks that can occur due to shrinkage significantly influence the safety and durability of concrete structures, it is important to identify cracks due to shrinkage in concretes that use blast furnace cement with a frost-resistant accelerator [16,17].

Thus, this study aims to identify the shrinkage and crack characteristics by conducting free shrinkage and restrained shrinkage tests on concretes that employ blast furnace cement and frost-resistant accelerator, and investigate changes in the shrinkage phenomenon focusing on the pore structure of the hardened cement paste and changes in the pore volume.

2. Experiment

2.1. Outline of experiment

Table 1 presents the experimental plan. The experiment employed a frost-resistant accelerator is inorganic nitrogenous compound of nitrite or nitrate, which consisted of only the frost-resistant component without including air-entraining (AE) or water-reducing components to investigate the sole effect of the frost-resistant accelerator in OPC and blast furnace cement Type B (hereafter referred to as BB) as a base cement with a 50% water–cement ratio (W/C). For the frost-resistant accelerator, 0% and standard usage 4% added four-level concretes were employed. The target slump and air content of the used concrete were 18 ± 2 cm and 4.5 ± 1.5%. Tables 2–4 present the used materials, binding materials properties and concrete mix designs.

Table 2
Materials Used.

Type	
Cement	Ordinary Portland cement, Density: 3.16 g/cm^3 Blast furnace slag cement, Blaine: 4000 cm^2/g, Density: 2.91 g/cm^3
Sand	Pit sand, Density: 2.67 g/cm^3, Absorption ratio: 1.57%
Gravel	Crushed aggregate, Density: 2.57 g/cm^3, Absorption ratio: 2.98%
Admixture	AE water reducing agent (Chemical compound with lignin sulphonic acid and polyol), Density: 1.23 ∽ 1.27 g/cm^3 Frost resistant accelerator (Main component: inorganic nitrogenous compound; Nitrite, Nitrate), Density: 1.41–1.45 g/cm^3, Amount of chloride ion: 0.01%

In addition, W/C 50% cement paste specimens were fabricated to evaluate the change in the shrinkage phenomenon according to the mix of the frost-resistant accelerator focusing on the pore structure and changes in pore volume.

2.2. Experiment method

Slump and air content immediately after pouring the concrete were measured to determine the properties of the fresh concrete.

The compressive strength was measured by fabricating a 100 × 200 mm cylinder specimen that was then demolded at one day old. Then, the compressive strength was measured at seven, 28, and 56 days under the standard water curing condition at 20 °C in accordance with ASTM C873/C873M-15 [18].

To determine the free shrinkage, a 100 × 100 × 400 mm prism specimen was used for demolding at one day old and water curing was conducted for seven days, and then the length change at a certain age was measured in accordance with ASTM C157/C157M-17 in the constant temperature and humidity chamber at 20 °C and 60% relative humidity (RH) conditions [19].

To determine the restrained shrinkage, restrained shrinkage strain due to the internal steel ring's restraint was measured when the height of the ring specimen was set to 75 mm from the 152 mm previously proposed by AASHTO (1998) to induce uniform dry shrinkage at the cross-section of the concrete ring, as shown in Fig. 1 [20,21]. A Teflon sheet was installed to prevent the restraint in the surface of the external ring and the specimen's lower side, and no surface treatment was applied to the restrained internal steel ring. The concrete surface was sealed using a vinyl sheet to prevent moisture evaporation that is a rapid drying phenomenon from the surface immediately after concrete pouring. At one day old, the wooden plate on the lower side of the ring specimen was demolded so that drying would only occur on the surfaces of the lower and upper concrete sides. A strain gauge was attached to three places in the center (h = 37.5 mm) of the internal steel ring to measure the restrained shrinkage strain using a data logger at constant temperature and humidity chamber at 20 °C and 60% RH conditions.

Table 1
Experimental Programs.

Specimen	BaseCement	Frost resistant accelerator (ml/c = 100 kg)	W/C (%)	Test items
OPC-0	Ordinary Portland Cement (OPC)	0	50	Slump
OPC-4		4		Air contents
BB-0	Blast Furnace Slag Cement (BB)	0		Compressive strength
BB-4		4		Free shrinkage
				Restraint shrinkage
				Archimedes method*
				Water vapor adsorption properties*

* Symbol marking was performed only on cement paste.

Table 3
Binding materials properties.

Binder	Specific surface area (g/cm^3)	Density (g/cm^3)	Chemical composition (%)							
			SiO_2	Al_2O_3	Fe_2O_3	CaO	MgO	SO_3	f-CaO	Ig.loss
OPC	3500	3.16	21.4	5.5	2.8	64.3	2.1	1.9	0.25	0.56
BFS	4000	2.91	34.0	14.4	0.83	43.3	6.5	–	–	0.1

Table 4
Mix designs of concrete.

Specimen	W/C (%)	s/a (%)	Unit Weight (kg/m^3)				AE water reducing agent (ml/C = 100 kg)	Frost resistant accelerator (ml/C = 100 kg)
			W	C	S	G		
OPC-0 OPC-4	50	44.8	178	356	764	965	250	0
BB-0 BB-4		44.9	174	349	769	965		4000

Target slump: 18 ± 2 cm, Target air contents: 4.5 ± 1.5%

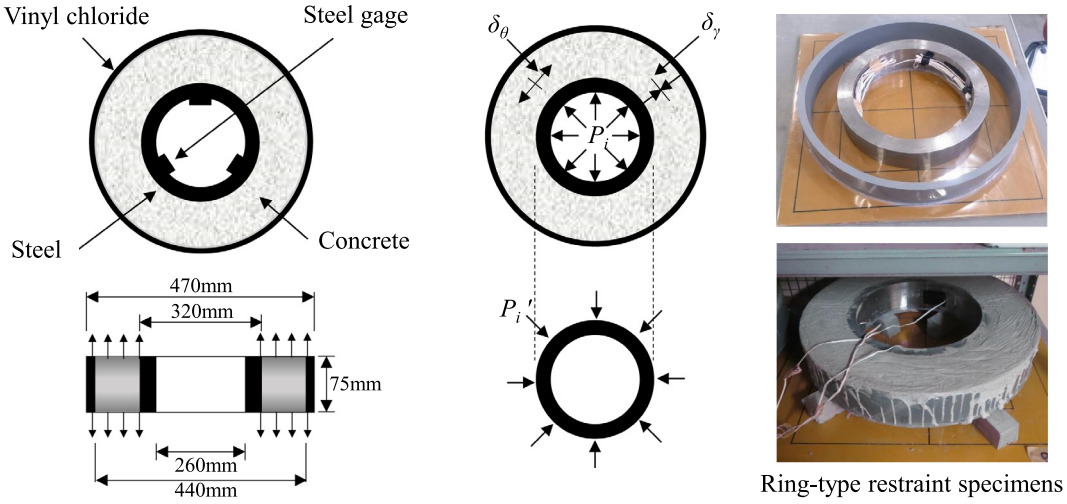

Fig. 1. Overview of the ring-type restraint test.

Meanwhile, changes in the pore volume in the pore section and ink bottle pore volume, which were considered to have a correlation with the shrinkage volume according to previous studies [22–25], were verified in the cement paste experiment. For the Archimedes method and mercury intrusion porosimetry (MIP) test as shown in Fig. 2, in order to obtain samples having possible representativeness for measurement of porosity, the specimens used in the analysis were cut into 5 mm cubes after collecting samples at predetermined ages and then drying was conducted for a week using hydration suspension and the D-dry method with ethanol substitution for a week. After this, the pore distribution was measured by the Archimedes method and MIP (Quantachrome PoreMaster 33). The pore diameter distribution up to the minimum diameter (6 nm) that was at the maximum pressure (220 MPa), was measured. In addition, a process in which mercury was intruded in the range 0.1–200 MPa and then depressurized to

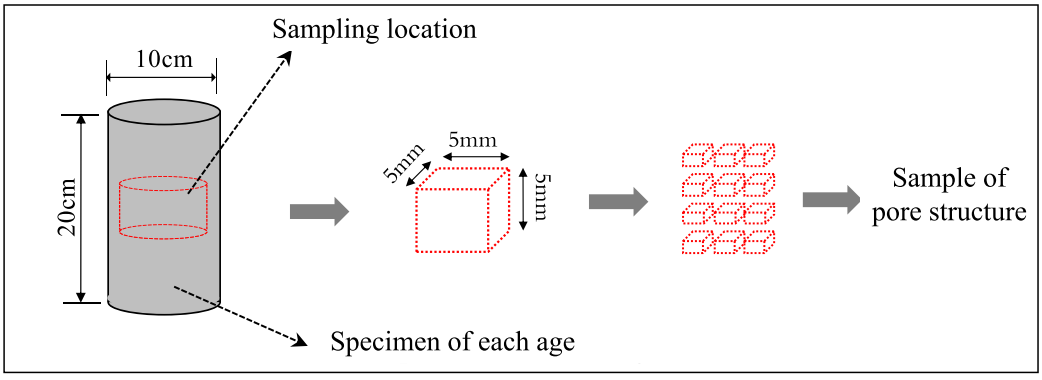

Fig. 2. Sampling of specimen for pore structure.

0.1 MPa to emit the mercury was conducted twice consecutively to calculate the mercury amount inside the pores and thus derive the ink-bottle pore volume based on the pore shape and continuity effects [22]. Three samples were collected per specimen of each case, and a total of three times repeat measurements were performed. As a result, three samples of each case showed almost the same void structure, and among them, one of the result was used for analysis.

3. Test results and discussion

3.1. Fresh and strength properties

Figs. 3 and 4 show the results of fresh concrete properties and compressive strength. The addition of the frost-resistant accelerator increases the amount of calcium aluminate-based hydrate (AFt) along with increases the consumption of water so that the slump of the concrete tends to decrease slightly. Also, since the frost-resistant accelerator used in this study was an accelerator that only consisted of the frost-resistant component without AE or water-reducing components, the slump tended to decrease slightly according to the frost-resistant accelerator content, but both the slump and air content satisfied the target performances. Therefore, it is considered that there is no significant change in the fresh properties in the range of the recommended amount of the frost-resistant accelerator. The compressive strength of OPC was larger than that of BB and the compressive strength of both OPC and BB increased from an early age as the frost-resistant accelerator was added, resulting in a significant increase to about 1.8–7.8 N/mm^2 compressive strength at 56 days old, which verified the hardening acceleration effect of the frost-resistant accelerator from an early age. The reaction rate of cement minerals such as aluminate (C_3A) and alite (C_3S) is increased at an early age, hydration is promoted with addition of the frost-resistant accelerator. As a result, it is considered that the setting time of the concrete is accelerated and the strength development of the concrete is also increased. Meanwhile, Strength improvement in BB in the long-term aging after 28 days was larger than that of the OPC due to the latent hydraulic activity.

3.2. Free shrinkage and restrained shrinkage

Figs. 5 and 6 show the results of the free shrinkage strain and mass change rate; the free shrinkage strains of OPC and BB were 680×10^{-6} and 805×10^{-6}, indicating that BB's shrinkage volume was 125×10^{-6} larger than that of OPC, which verified the general trend. When the frost-resistant accelerator was mixed, the shrinkage volume of BB-4 at 56 days old was similar to that of BB-0, but that of OPC-4 was 62×10^{-6} larger than that of OPC-0, indicating that the shrinkage volume of both OPC and BB had increased by $50–100 \times 10^{-6}$ from that of the early age overall as the frost-resistant accelerator was added. In contrast, the result of the mass change rate exhibited no general trend; the larger the mass change rate, the larger the length change rate. That is, this test results

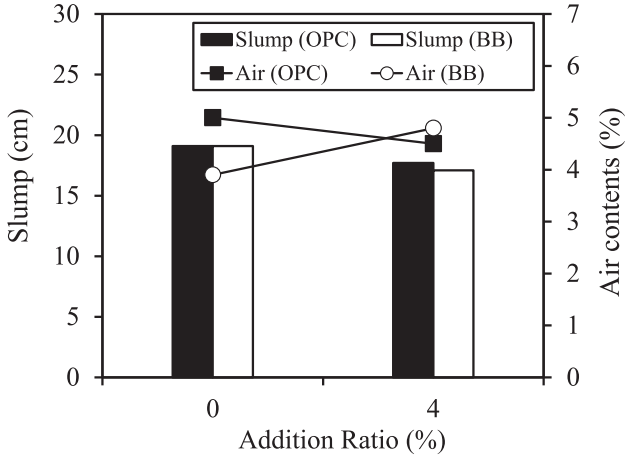

Fig. 3. Slump and air content.

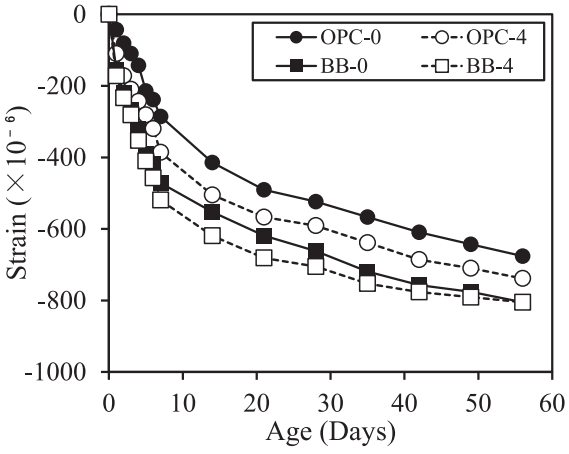

Fig. 5. Free shrinkage.

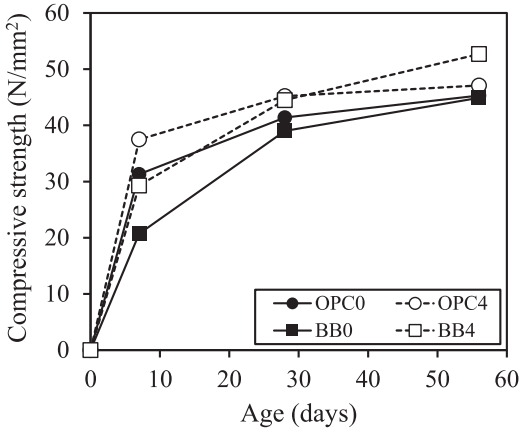

Fig. 4. Compressive strength.

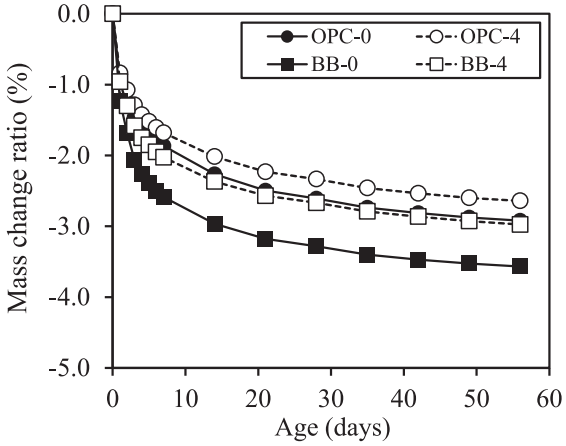

Fig. 6. Mass change rate.

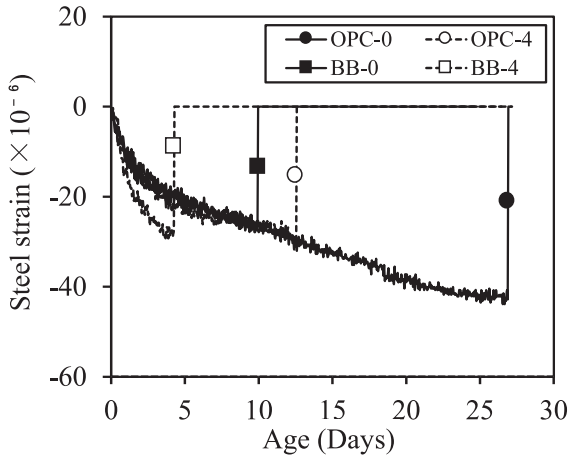

Fig. 7. Restrained shrinkage.

showed that the frost-resistant accelerator-added specimen that had the largest shrinkage volume exhibited the smallest mass change rate. As mentioned above, this was because, the addition of the frost-resistant accelerator increases the reaction rate of aluminate (C_3A) and alite (C_3S) at an early ages, it increases the amount of calcium aluminate-based hydrate (AFt), at the same time, increases the consumption of water, thereby the setting time is accelerated, and making the moisture evaporation to the outside small. However, it is considered that the pore structure or pore distribution inside the concrete may also affect the shrinkage characteristics, and further investigation is needed in the future.

Fig. 7 shows the restrained shrinkage strain results for the ring test. The restrained shrinkage strain increased gradually as the in free shrinkage strain increased and the specimen aged, thereby developing through-wall cracks after the maximum strain. The time when the restrained shrinkage strain reached zero was the occurrence day of cracks for each specimen. Table 5 presents the crack shape and crack occurrence days. BB-4 had the fastest crack occurrence followed by BB-0, OPC-4, and OPC-0, indicating that cracks were generated earlier in BB than in OPC. The results verified that the frost-resistant accelerator-added specimens also had faster crack occurrence dates as the free shrinkage strain increased.

3.3. Restraint stress and cracking potential

The restraint tensile stress can be calculated by Eq. (1) using the radiuses of the concrete and steel ring, restrained shrinkage strain, and the elastic modulus of the steel ring assuming that the concrete poured in the ring specimen had uniform shrinkage in the shear plane with linear behavior [26–28].

$$\sigma_{max} = \frac{(r_{os^2} - r_{is^2})}{2r_{os^2}} \cdot \frac{(r_{im^2} + r_{om^2})}{(r_{om^2} - r_{im^2})} \cdot E_{st} \cdot \varepsilon_{st} \quad (1)$$

Here, σ_{max} refers to the restraint tensile stress, r_{is} and r_{os} refer to internal and external radii of the steel ring, r_{ic} and r_{oc} refer to the internal and external radii of the concrete, E_{st} refers to the elastic modulus, and ε_{st} refers to the restrained shrinkage strain.

Fig. 8 shows the restraint tensile stress calculated by Eq. (1). The restraint tensile stress increased as the restrained shrinkage strain increased and then cracks occurred after the maximum restraint tensile stress at approximately 3.1–3.9 N/mm^2. As the frost-resistant accelerator was mixed, the restraint tensile stress increased due to the increase in pressure generated in the internal steel ring in the case of both of OPC and BB; accordingly, cracks in the concrete occurred rapidly. The cause of the above result was

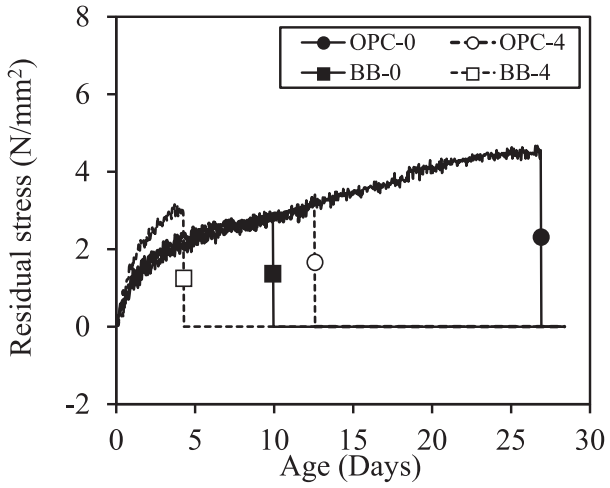

Fig. 8. Restraint tensile stress.

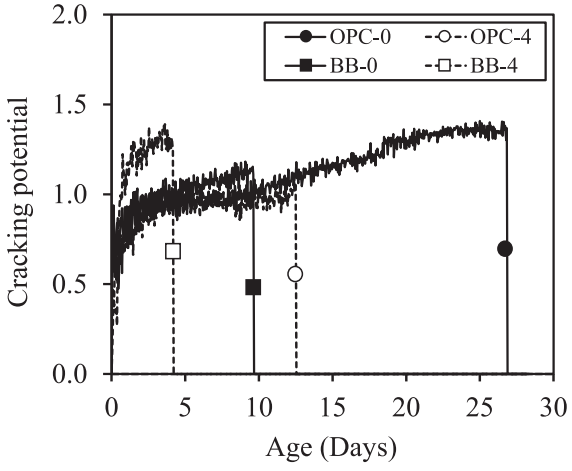

Fig. 9. Cracking potential.

Table 5
Crack configuration and cracking days.

Specimen	OPC-0	OPC-4	BB-0	BB-4
Cracking				
Days of cracking	26.88	12.54	9.92	4.25

because the restraint tensile stress at the same age tended to increase as the frost-resistant accelerator was mixed in. In the same manner, when the frost-resistant accelerator was mixed, the strain of the internal steel ring increased due to the increase in the free shrinkage strain from an early age, which was why the stress relaxation was reduced by the tensile creep. Meanwhile, the cracking potential was a ratio of the restraint tensile stress/tensile strength, which was calculated by the stress-to-strength ratio, and the tensile strength was calculated by Eq. (2) using the results of the compressive strength [21,29].

$$\sigma_{tensile} = 0.291 \cdot F_c^{0.658} \cdot \varepsilon_{st} \quad (2)$$

Here, $\sigma_{tensile}$ refers to the tensile strength and F_c refers to the compressive strength.

Fig. 9 shows each specimen's cracking potential. The cracking potential of BB was larger than that of OPC. The figure verified that as the frost-resistant accelerator was added, the cracking potentials of both OPC and BB tended to increase. Based on the results of OPC-4 and BB-4 (which showed faster crack occurrence date for each cement), the crack occurrence possibility due to shrinkage was increased by 12% for OPC and 21% for BB within the range of the restraint condition in this test as the frost-resistant accelerator was added.

3.4. Pore structure

The pore area, which was regarded as correlating with the shrinkage volume, was investigated with regard to the cement paste specimen. Fig. 10 shows the total void ratios of the cement pastes according to the Archimedes method. The figure verified that as the age increased, the total void ratio tended to decrease, and the total void ratio tended to decrease as the frost-resistant accelerator was added. Adding the frost-resistant accelerator increased the production of hydration products due to the hydration acceleration from an early age, thereby making the pore structure denser. Fig. 11 shows the pore distribution of the cement pastes using mercury intrusion porosimetry. When the frost-resistant accelerator was not added, OPC tended to become denser than BB. When the frost-resistant accelerator was added, the movement of the pore size peak to the denser side was verified in both OPC and BB.

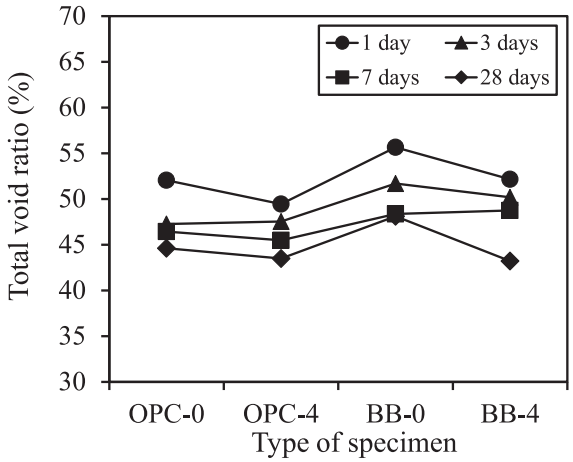

Fig. 10. Total void ratio.

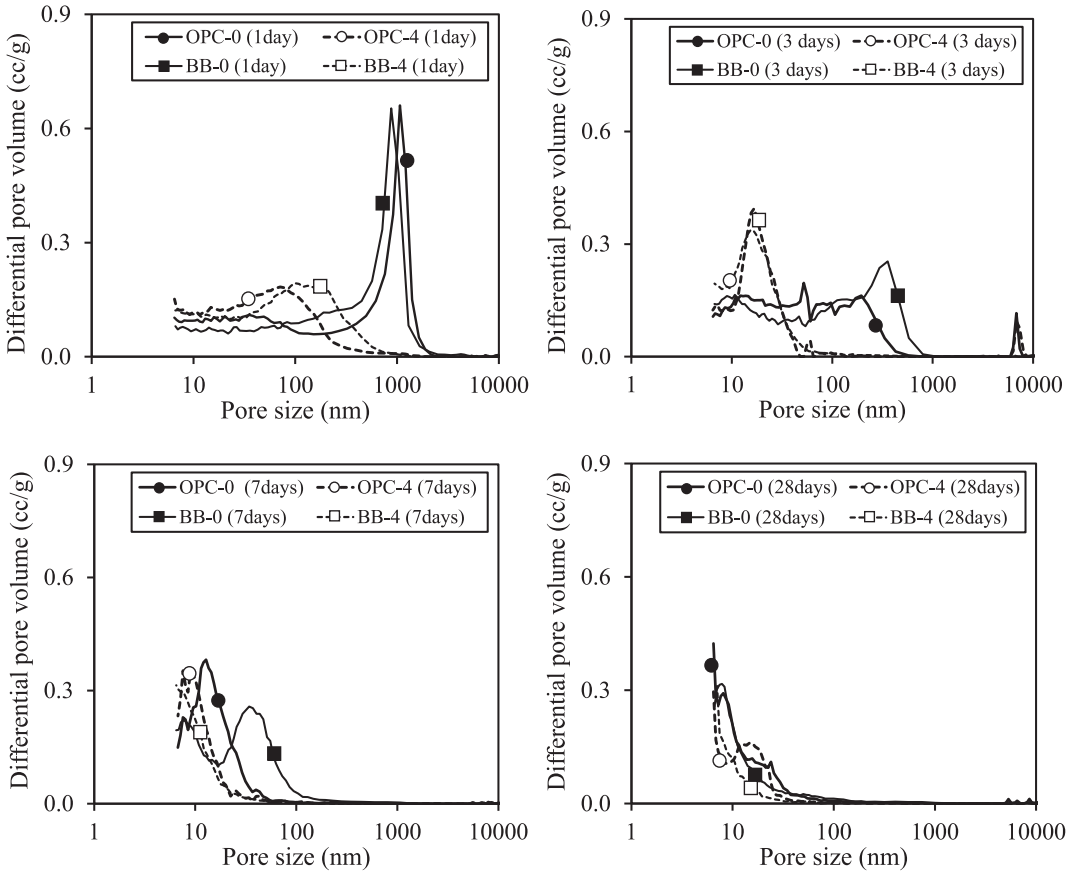

Fig. 11. Pore distribution.

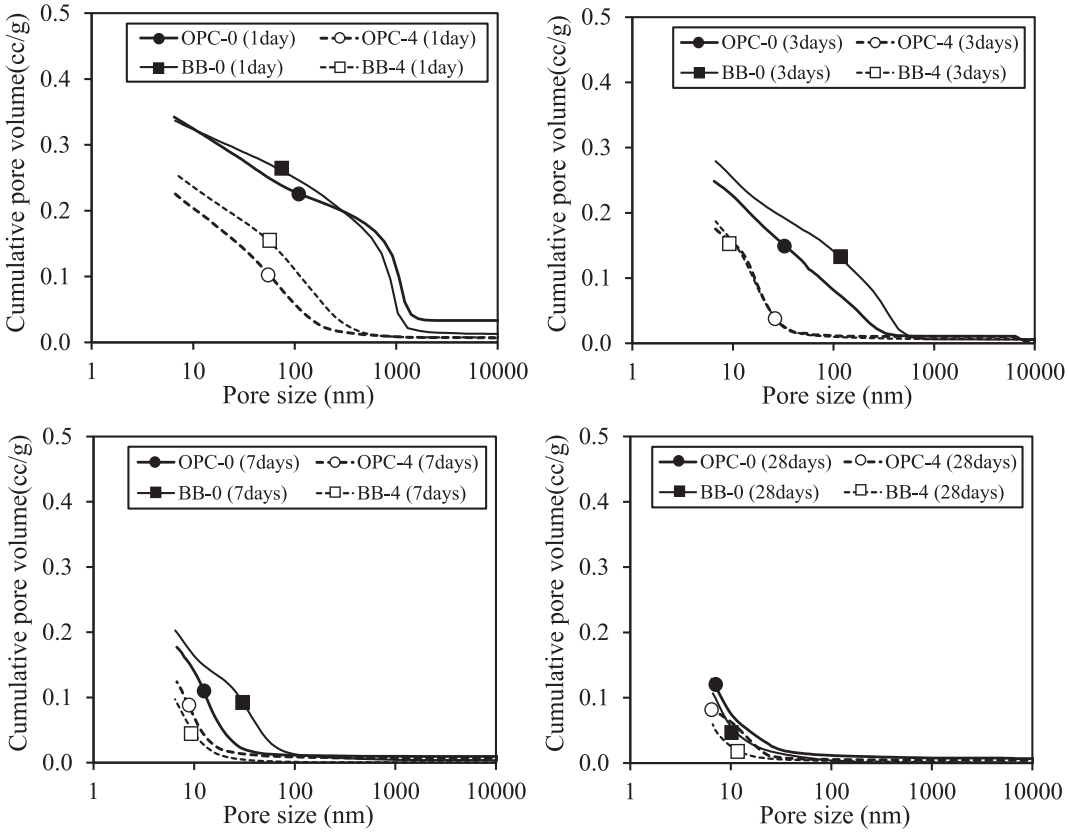

Fig. 12. Cumulative pore volume.

Fig. 12 shows the cumulative pore volume of the cement paste. At the same as the results for the total void ratio, denser pores were verified due to the addition of the frost-resistant accelerator and as the cement aged. The cumulative pore volume had a large difference depending on whether the frost-resistant accelerator was added at the early age. However, the difference diminished as the age increased. Thus, the difference due to cement type and the presence of frost-resistant accelerator was reduced at 28 days and the hardening acceleration effect of the frost-resistant accelerator was verified at the early age.

3.5. Relationship between pore structure and shrinkage

The correlation of the measurement results at 28 days obtained from the drying shrinkage test for the concrete specimen with pore structure obtained by the Archimedes method and mercury intrusion porosimetry in the cement paste test were investigated based on the previous study results [22,23]. Generally, a pore size that affects the drying shrinkage of cement-based materials was known to be 30 nm diameter or smaller within the range 55–60% RH. In particular, previous study results reported that a pore volume <8 nm in diameter influenced the drying shrinkage of hardened cement paste [22,23]. Thus, this study also investigated the relationship between the length change and pore volume <30 nm in diameter and the pore volume <8 nm in diameter at 28 days.

The measurable pore size by mercury intrusion porosimetry in this test was ≥6 nm diameter. Thus, the pore distribution of <6 nm diameter could not be measured. Accordingly, the pore volume of <6 nm diameter was calculated by subtracting the pore volume ≥6 nm diameter obtained by the mercury intrusion porosimetry from the total void ratio obtained by the Archimedes method. Considering this, the pore volumes for <30 nm and <8 nm diameter were calculated [22]. Figs. 13 and 14 show the correlations between the length change rate and pore volume <30 nm diameter, and the pore volume <8 nm diameter, respectively. Both OPC and BB verified that the pore volume <30 nm diameter and the pore volume <8 nm diameter were decreased, and the shrinkage increased as the frost-resistant accelerator was mixed. In particular, it verified the high correlation between the length change and pore volume <30 nm diameter.

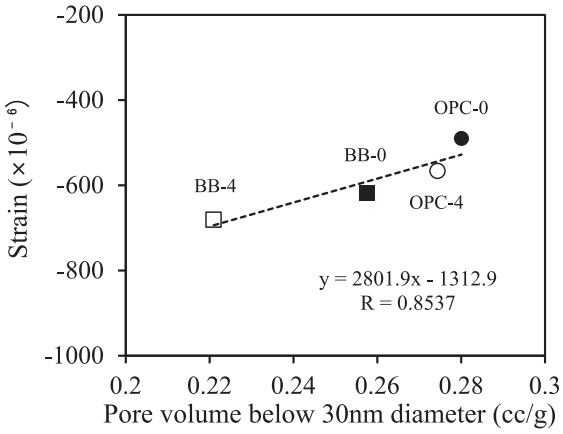

Fig. 13. Correlations between the length change and pore volume < 30 nm diameter.

In addition, the pore distribution <30 nm diameter was divided into Min. (0–20 nm) and Max. (6–30 nm) and the correlation between pore volume and length change in each section was examined to determine that the range of pore size that correlated with the length change was large according to the addition of the

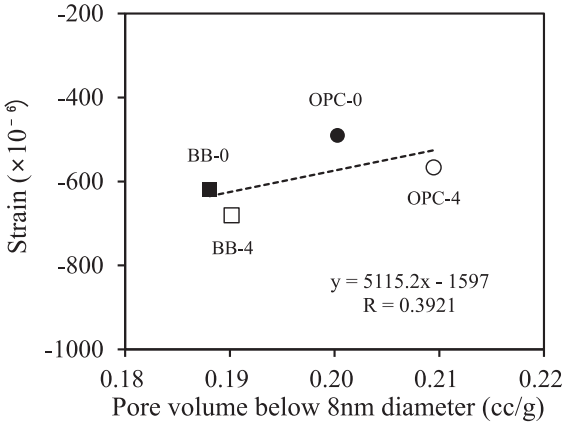

Fig. 14. Correlations between the length change and pore volume < 8 nm diameter.

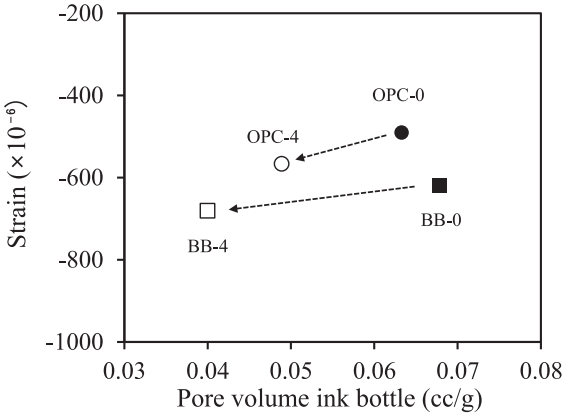

Fig. 16. Relationship between ink-bottle pore volume and length change.

frost-resistant accelerator. Table 6 presents the coefficient of determination of pore volume and length change for each section. In the sections set in this study, the coefficient of determination between pore volume <20–30 nm diameter and length change was verified as the highest (0.9942). Thus, as the frost-resistant accelerator was added, the pore volume <30 nm in diameter; in particular, the pore volume <20–30 nm diameter affected the length change the most, as shown in Fig. 15.

Fig. 16 shows the relationship between ink-bottle pore volume and length change. Previous studies have investigated moisture movement inside the ink-bottle pore, and their studies reported that shrinkage was reduced by the redistribution of moisture inside the ink-bottle into the inside as moisture drying progressed at the ink-bottle inlet [24,25]. This study verified the shrinkage-reducing effect of the ink-bottle pore since the ink-bottle pore volume was reduced by the addition of the frost-resistant accelerator regardless of cement type (OPC and BB), which was because the shrinkage increased as the frost-resistant accelerator was added.

Table 6
Relationship between pore size and drying shrinkage.

Min.	Max.			
	6 nm	10 nm	20 nm	30 nm
0 nm	0.1092	0.8193	0.7707	0.8537
6 nm	–	0.0812	0.595	0.707
10 nm	–	–	0.6531	0.8144
20 nm	–	–	–	0.9942

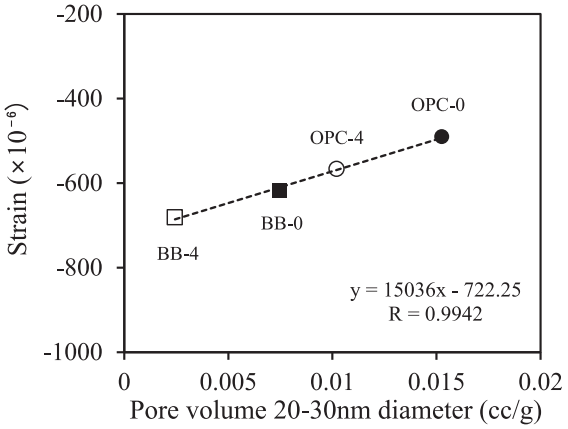

Fig. 15. Correlations between the length change and pore volume < 20–30 nm diameter.

The above results show that the pore structure, particularly the pore volume and ink-bottle pore volume <20–30 nm diameter were reduced as the frost-resistant accelerator was added to both OPC and BB, thereby verifying that the length change increased, and the change in the pore volume in this range was found to significantly affect the shrinkage properties of the frost-resistant accelerator-added hardened cement paste.

4. Conclusion

This study investigated the shrinkage properties of concrete using blast furnace cement with a frost-resistant accelerator, and the study results obtained the following conclusions.

(1) The frost-resistant accelerator content had a small effect on the fresh concrete properties. In addition, the compressive strength of both OPC and BB increased from an early age as the frost-resistant accelerator was added, thereby verifying the hardening acceleration effect of the frost-resistant accelerator at the early age.
(2) The free shrinkage strain of both OPC and BB increased from an early age as the frost-resistant accelerator was mixed, and this study verified that the cracks tended to occur rapidly under the restraint condition. In particular, the cracking potential of both OPC and BB tended to increase as the frost-resistant accelerator was mixed, and the results verified that the cracking potentials of OPC and BB were increased by approximately 12% and 21%, respectively.
(3) The study results verified that the change in length of both of OPC and BB tended to increase when adding the frost-resistant accelerator. This was due to the change in pore volume <30 nm in diameter; in particular, the reduction in pore volume <20–30 nm diameter and ink-bottle pore volume as the frost-resistant accelerator, and the change in pore volume in this range was deemed to have a large effect on the shrinkage properties of the frost-resistant accelerator-added hardened cement paste.

Conflict of interest

None.

Acknowledgments

This work was supported by the National Research Foundation of Korea (NRF) grant funded by the Korea government (MSIT) (No. NRF-2018R1A5A1025137).

References

[1] D. Tsuji, M. Kojima, M. Kuroda, N. Sakata, Study on the basic properties of concrete using high amount of ground-granulated blast-furnace slag, Proc. Japan Concr. Inst. 35 (1) (2013) 145–150.
[2] T. Yonezawa, E. Sakai, K. Koibuchi, M. Kinoshita, High-slag cement and structures for substantial reduction of energy CO_2, in: Proceedings, fib Symposium Stockholm, 2012, pp. 463–466.
[3] S. Tamaki, K. Saito, K. Okada, D. Atarashi, E. Sakai, Properties of a new type of polycarboxylate admixture for concrete using high volume blast furnace slag cement, Special Publ. 302 (2015) 113–124.
[4] AIJ, Recommendation for practice of concrete with Portland cement and ground granulated blast-furnace, Slag: Archit. Inst. Japan (2001).
[5] KCI, Guide Specification for Concrete Work - Cold Weather Concreting, Korea Concrete Institute of Japan, 2016.
[6] AIJ, Recommendation for Practice of Cold Weather Concreting, Architectural Institute of Japan, 2010.
[7] A.C.I. Committee, 306, Guide to Cold Weather Concreting, American Concrete Institute, 2010.
[8] ACI 306.1-90, Standard Specification for Cold Weather Concreting, (2002) 1–5.
[9] M. Taniguchi, T. Nakamura, S. Koike, H. Nishi, Study on Effect and Mechanism of Accelerator for Freeze Protection, Hokkaido Research Organization Northern Regional Building Research Institute (Research report), 2015, pp. 1–11.
[10] Y. Hama, E. Kamada, The properties of concrete containing a frost-resistant accelerator, Concr. J. 37 (11) (1999 Jan) 3–8.
[11] Yukio Hama, Eiji Kamada, Strength development under freezing conditions and freezing behavior of water in concrete with accelerators for freeze protection, Concr. Res. Technol. 8 (2) (1997) 73–80.
[12] C.K. Nmai, Cold weather concreting admixtures, Cem. Concr. Compos. 20 (1998) 121–128.
[13] R. Polat, F. Karagol, R. Demirboga, M.A. Kaygusuz, M.M. Yadollahi, The influence of calcium nitrate as antifreeze admixture on the compressive strength of concrete exposed to low temperatures, Cold Reg. Sci. Technol. 89 (2013) 30–35.
[14] Frost-Resistant Accelerator Operational Manual. Ministry of Land, Infrastructure and Transport. Japan; 2005. 1-7
[15] Y. Nonomura, A. Shimata, H. Shimada, S. Yoshida, Fundamental Study for Expansion of use of Frost-Resistant Accelerator for Blast Furnace Slag Cement Monthly report, Civil Engineering Research Institute for Cold Region, 2015, pp. 45–50.
[16] AIJ, Recommendations for Practice of Crack Control in Reinforced Concrete Buildings (Design and Construction), Architectural Institute of Japan, Tokyo, 2006, pp. 17–24.
[17] JCI, Research Committee Report on Shrinkage of Concrete, Japan Concrete Institute, Tokyo, 2010, pp. 81–82.
[18] ASTM C873/C873M-15, Standard Test Method for Compressive Strength of Concrete Cylinders Cast in Place in Cylindrical Molds, ASTM International, West Conshohocken, PA, 2015.
[19] ASTM C157/C157M-17, Standard Test Method for Length Change of Hardened Hydraulic-Cement Mortar and Concrete, ASTM International, West Conshohocken, PA, 2017.
[20] American Association of State Highway and Transportation Officials. Standard Practice for Estimating the Crack Tendency of Concrete. 1998: 34-99
[21] H.G. Choi, M.K. Lim, R. Kitagaki, T. Noguchi, G.Y. Kim, Restrained shrinkage behavior of expansive mortar at early ages, Constr. Build. Mater. 84 (2015) 468–476.
[22] R. Narumi, W. Zhang, Y. Kishimoto, Y. Hama, Investigation of affecting factors on reductance of drying shrinkage and degradation of frost resistance of mortar with shrinkage reducing agent, J. Struct. Constr. Eng. (Transactions of AIJ). 72 (700) (2014 Jul) 671–680.
[23] C.G.J. Maria, M.J. Hamlin, Examining the relationship between the microstructure of calcium silicate hydrate and drying shrinkage of cement paste, Cem. Concr. Res. 32 (2) (2002 Feb) 289–296.
[24] O.K. Knut, H.A. Elisabeth, Pore structure of cement silica fume systems presence of hollow-shell pores, Cem. Concr. Res. 29 (1999 Jan) 133–142.
[25] M.E. Rosa, F. Lutz, Influence of the age and drying process on pore structure and sorption isotherm of hardened cement paste, Cem. Concr. Res. 36 (2006 Oct) 1969–1984.
[26] A.B. Hossain, W.J. Weiss, Assessing residual stress development and stress relaxation in restrained concrete ring specimens, Cem. Concr. Compos. 26 (5) (2004) 531–540.
[27] W.J. Weiss, S. Fergeson. Restrained Shrinkage Testing: The Impact of Specimen Geometry on Quality Control Testing for Material Performance Assessment: Concreep 6, Creep, Shrinkage, and Durability Mechanic of Concrete and other Quasi-Brittle Materials. Ulm FJ, Bazant ZP, and Wittman FH, eds., Elsevier, Cambridge MA. 2001: 645-651.
[28] A.C. Ugural, S.K. Fenster, Advanced Strength and Applied Elasticity ISBN 0-137589-X, third ed., Prentice Hall PTR, 1995.
[29] T. Noguchi, F. Tomozawa, Relationship between compressive strength and various mechanical properties of high strength concrete, J. Struct. Constr. Eng. 472 (1995) 11–16.